Piezoelectric Disk Gyroscope Fabricated With Single-Crystal Lithium Niobate

AUTHOR(S):

Obitani, Kazutaka; Araya, Kazutaka; Yachi, Masanori; Tsuchiya, Toshiyuki

CITATION:

Obitani, Kazutaka ...[et al]. Piezoelectric Disk Gyroscope Fabricated With Single-Crystal Lithium Niobate. Journal of Microelectromechanical Systems 2021, 30(3): 384-391

ISSUE DATE:

2021-06

URL:

http://hdl.handle.net/2433/284805

Piezoelectric Disk Gyroscope Fabricated with Single-Crystal Lithium Niobate

Kazutaka Obitani, Kazutaka Araya, Masanori Yachi, Toshiyuki Tsuchiya, *Member, IEEE*

***Abstract*— A piezoelectric disk gyroscope fabricated with a single-crystal lithium niobate (LN) wafer has been developed for inertial navigation systems for localization during automated driving. LN has a high electromechanical coupling coefficient and a resonator made of a low-cost single-crystal wafer shows a high quality factor, which is suitable for high-performance vibratory gyroscopes. In this study, its crystallographic anisotropies in both in elastic and piezoelectric properties were considered to realize mode matching in the two-wine-glass-mode vibration of a disk resonator. We chose a 155°-Y-cut LN wafer because we found that its elastic compliance is uniform in any in-plane direction. Its anisotropic piezoelectric properties were considered to optimize the electrode design to oscillate the wine-glass modes efficiently. A 25.8-mm-diameter, 330-µm-thick disk resonator with 16 electrodes on each side was designed and fabricated by photolithography and grinding. The as-fabricated LN disk resonator was successfully oscillated in two wine-glass modes with a small frequency split of 0.7% at 95 kHz resonant frequency. Gyroscope operation was successful and the scale factor was 0.35 µV/°/s without any preamplifier.**

***Index Terms*— Disk resonator, Lithium niobate, Piezoelectric transducers, Single crystal, Vibratory gyroscope.**

I. Introduction

AUTONOMOUS DRIVING TECHNOLOGY requires high-performance inertial sensors for accurate navigation, smooth steering, and attitude control. A gyroscope detects the angular rate of an object, and for automotive driving control, it detects the position and angle of its body with an accelerometer to maintain automated control without external positioning information from, for example, global positioning system and image sensors. For the automobile localization system, the bias stability should be less than 0.1°/h for the positioning accuracy of 0.1 m on highway driving. A fiber optical gyroscope and a ring laser gyroscope have been used for demonstrating such automated driving [1]. However, these types of gyroscopes which are mainly for aerospace applications, are too expensive to adopt to automobiles. Therefore, there is a strong demand to improve the performance of microelectromechanical system(MEMS)-based gyroscopes. Although state-of-the-art MEMS gyroscope in research papers [2, 3] has the bias instability of less than 1°/h, it is still difficult to make such a device into a product with a reasonable price.

In MEMS Coriolis vibratory gyroscopes (CVGs) consisting of at least two-degree-of-freedom vibrating systems, their performance will be better if the electromechanical coupling coefficient and quality factor (Q) are high. With a high Q value, the signal to noise ratio will be high, because the output signal is large even if the actuation input signal is small. These values also affect the vibration stability, which results in the better bias instability. Piezoelectric quartz [4] and electrostatic silicon CVGs [5, 6] show a high Q of more than 100,000 because of their single crystalline nature. Since their electromechanical coupling coefficient is relatively low, much effort has been devoted for improving the Q factor [7-10]. Piezoelectric ceramics (such as lead titanate zirconate) have a high coupling coefficient, but their Q is not high because of loss caused by grain boundaries [11, 12].

Table 1 Gyroscope materials

	Electrostatic		Piezoelectric	
	Silicon [5]	Quartz [4]	PZT [7, 8]	LN [9, 10]
K	Low < 0.1%	Midium 1 ~ 10%	High ~ 70%	High 30 ~ 70%
Q	Very high > 100,000	High > 10,000	Low ~ 1,000	High > 10,000

Lithium niobate ($LiNbO_3$, LN) is a trigonal ilmenite single-crystal piezoelectric material belonging to the 3m crystal point group [13] and it shows a high Q of more than 10,000 and an electromechanical coupling coefficient of up to 30–70% [14]. As summarized in Table 1, although the Q value is smaller than silicon, the coupling coefficient of LN is much higher. LN vibratory gyroscope has a potential of better S/N ratio at comparable bias instability compared to silicon ones. Using single crystal LN, tuning-fork-type [15] and shear-deformation-type [16] CVGs have been developed. However, owing to their poor workability and low dry and chemical etching rates, it is

This research is supported by Adaptable and Seamless Technology transfer Program through Target-driven R&D (A-STEP: JPMJTM19YP) from JST and Kyoto University Nanotechnology Hub in the "Nanotechnology Platform Project" sponsored by MEXT, Japan.

K. Obitani was with Kyoto University, Kyoto 6158540 Japan. He is now with Sumitomo Electric Industries, Ltd., Osaka, Japan (e-mail: k_obitani@nms.me.kyoto-u.ac.jp).

K. Araya is with Tamagawa Seiki. Co. Ltd.., Hachinohe, Aomori 0392245, Japan. (e-mail: kazutaka-araya@tamagawa-seiki.co.jp).

M. Yachi is with Tamagawa Mobile Equipment Co. Ltd., Hachinohe, Aomori 0392245, Japan. (e-mail: masanori-yachi@tme.tamagawa-seiki.co.jp).

T. Tsuchiya is with the Department of Micro Engineering, Kyoto University, Kyoto 6158540, Japan (e-mail: tutti@me.kyoto-u.ac.jp).

difficult to fabricate complicated mechanical structures. The current performance of tuning-fork-type LN CVGs is not better than current silicon-based CVGs.

To improve their performance, wine-glass-mode disk [5, 17–20], ring [6], and hemispherical [21, 22] resonators have been used owing to their structural symmetry. These resonators use elliptical vibration in two orthogonal wine-glass modes for driving and detection, and operate by matching the resonance frequencies of the two vibration modes (mode matching). The mode-matching is especially needed for high-performance operating modes, such as a force-rebalanced mode [23, 24], frequency modulated mode [25, 26], and whole-angle mode [19, 27-30]. However, single-crystal LN has anisotropic properties, not only properties but also piezoelectric properties. Therefore, it is difficult to realize mode-matched gyroscopes using LN disk resonators.

In this study, we developed a disk vibratory gyroscope using LN, which is available as a single-crystal wafer at a reasonable price. To mitigate the anisotropy of elastic properties of LN, we investigated the best crystal orientation for a wine-glass mode resonator, at which the elastic compliance is uniform for any in-plane direction. In addition, the piezoelectric constant of the orientation is considered and the optimized electrode design is proposed. The fabrication process using grinding process is proposed and the device was fabricated. The rate output of the fabricated disk resonator with closed-loop oscillation and open-loop detection is presented in this paper.

II. Design

The operation principle of a disk vibratory gyroscope [31] is shown in Fig. 1. Two wine-glass modes, the 0° mode and 45° mode, are used for driving and sensing. In this work, the 45° mode is used for driving mode and the 0° mode is for sensing mode. The Coriolis force from rotation about the 3-axis oscillates the sensing mode vibration, and its vibration amplitude is proportional to the angular rate and detected by a demodulator.

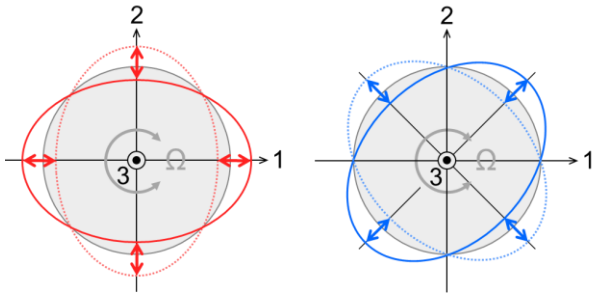

Figure 1: Operation principle of disk vibratory gyroscope. (a) 0° wine-glass mode. (b) 45° wine-glass mode.

It is important that the two modes are closely matched and the Q values are high for a high-performance gyroscope [23]. Therefore, the disk should have a symmetrical shape and isotropy in its elastic property. The in-plane compliances for the plane perpendicular to the 3-axis should be constant for any direction.

A. *Wafer orientation [32]*

To achieve mode matching in two wine-glass modes using single-crystal LN wafers, we searched the optimum crystal orientation where elastic compliances at about one and two axes are constant in any in-plane orientation.

The piezoelectric constants are defined with the *XYZ* coordinate system, where the *Z*-axis is the polarized axis (crystalline *XYZ* coordinate system). In this paper, a wafer coordinate system of *X''Y''Z''* is defined by rotating the *XYZ* coordinate system with an angle ψ about the *Z*-axis and then by rotating the *X'Y'Z'* coordinate system with an angle θ about the *X'*-axis in accordance with the definition of Euler angles (Fig. 2).

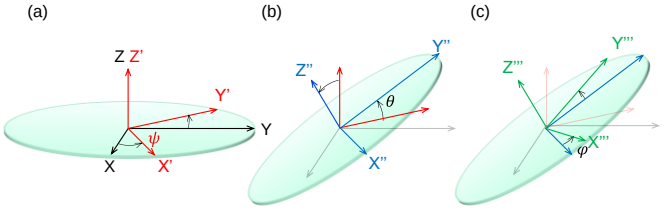

Figure 2: Definition of Euler angles. (a) rotation around Z-axis, (b) rotation around X'-axis, (c) rotation around Z''-axis.

In the crystalline *XYZ* coordinate system, the relationship between strain S and stress T for 3m crystals is given as

$$\begin{pmatrix} S_1 \\ S_2 \\ S_3 \\ S_4 \\ S_5 \\ S_6 \end{pmatrix} = \begin{bmatrix} s_{11} & s_{12} & s_{13} & s_{14} & 0 & 0 \\ s_{12} & s_{11} & s_{13} & -s_{14} & 0 & 0 \\ s_{13} & s_{13} & s_{33} & 0 & 0 & 0 \\ s_{14} & -s_{14} & 0 & s_{44} & 0 & 0 \\ 0 & 0 & 0 & 0 & s_{44} & 2s_{14} \\ 0 & 0 & 0 & 0 & 2s_{14} & 2(s_{11}-s_{12}) \end{bmatrix} \begin{pmatrix} T_1 \\ T_2 \\ T_3 \\ T_4 \\ T_5 \\ T_6 \end{pmatrix}, \quad (1)$$

where s indicates elastic compliance components [13, 33]. Equation (1) can be written in the wafer coordinate system as

$$\begin{pmatrix} S_1'' \\ S_2'' \\ \cdot \\ \cdot \\ \cdot \\ S_6'' \end{pmatrix} = \begin{bmatrix} s_{11}'' & s_{12}'' & \cdot & \cdot & \cdot & s_{16}'' \\ s_{12}'' & s_{22}'' & \cdot & \cdot & \cdot & s_{26}'' \\ \cdot & \cdot & \cdot & \cdot & \cdot & \cdot \\ \cdot & \cdot & \cdot & \cdot & \cdot & \cdot \\ \cdot & \cdot & \cdot & \cdot & \cdot & \cdot \\ s_{16}'' & s_{26}'' & \cdot & \cdot & \cdot & s_{66}'' \end{bmatrix} \begin{pmatrix} T_1'' \\ T_2'' \\ 0 \\ 0 \\ 0 \\ T_6'' \end{pmatrix}. \quad (2)$$

Here, it is assumed that the disk is thin and under plane stress. Therefore, the stress components T_3, T_4, T_5 are zero and the components shown as dots in the compliance matrix can be neglected. In order to check in-plane compliance isotropy of the rotated coordinate, the *X''Y''Z''* coordinate system is rotated in-plane by an angle φ about the *Z''*-axis. The rotated elastic compliance components s'' in Eq. (2) can be rewritten in the *X'''Y'''Z'''* coordinate system as,

$$\begin{cases} s_{11}''' = \frac{1}{8}(s_{11}'' - 2s_{12}'' + s_{22}'' - s_{66}'')\cos 4\varphi + \frac{1}{4}(s_{16}'' - s_{26}'')\sin 4\varphi \\ \quad + \frac{1}{2}(s_{11}'' - s_{22}'')\cos 2\varphi + \frac{1}{2}(s_{16}'' + s_{26}'')\sin 2\varphi \\ \quad + \frac{1}{8}(3s_{11}'' + 2s_{12}'' + 3s_{22}'' + s_{66}'') \\ s_{12}''' = -\frac{1}{8}(s_{11}'' - 2s_{12}'' + s_{22}'' - s_{66}'')\cos 4\varphi - \frac{1}{4}(s_{16}'' - s_{26}'')\sin 4\varphi \\ \quad + \frac{1}{8}(s_{11}'' + 6s_{12}'' + s_{22}'' - s_{66}'') \\ s_{16}''' = \frac{1}{2}(s_{16}'' - s_{26}'')\cos 4\varphi - \frac{1}{4}(s_{11}'' - 2s_{12}'' + s_{22}'' - s_{66}'')\sin 4\varphi \\ \quad + \frac{1}{2}(s_{16}'' + s_{26}'')\cos 2\varphi - \frac{1}{2}(s_{11}'' - s_{22}'')\sin 2\varphi \\ s_{66}''' = -\frac{1}{2}(s_{11}'' - 2s_{12}'' + s_{22}'' - s_{66}'')\cos 4\varphi - (s_{16}'' - s_{26}'')\sin 4\varphi \\ \quad + \frac{1}{2}(s_{11}'' - 2s_{12}'' + s_{22}'' + s_{66}''). \end{cases} \quad (3)$$

These components are not affected by the neglected components in Eq. 2. It is desired that s_{11}''', s_{12}''', s_{16}''', and s_{66}''' are independent from φ. That is, the coefficients of trigonometric function should be almost zero. s_{22}''' and s_{26}''' do not need to be considered because they are equivalent to s_{11}''' and s_{16}''', respectively. According to eq. (3), there are four independent parameters, $s_{11}'' - 2s_{12}'' + s_{22}'' - s_{66}''$, $s_{16}'' - s_{26}''$, $s_{11}'' - s_{22}''$, and $s_{16}'' + s_{26}''$. Since s_{11}''' contains all of them, we defined an evaluation function of s_{11}''', coefficient of variation $C.V.(\psi,\theta)$, as

$$C.V.(\psi,\theta) = \frac{\sqrt{\frac{1}{2}a_4^2 + \frac{1}{2}b_4^2 + \frac{1}{2}a_2^2 + \frac{1}{2}b_2^2}}{a_0},$$
$$\text{where} \quad a_4 = (s_{11}'' - 2s_{12}'' + s_{22}'' - s_{66}'')/8$$
$$b_4 = (s_{16}'' - s_{26}'')/4$$
$$a_2 = (s_{11}'' - s_{22}'')/2$$
$$b_2 = (s_{16}'' + s_{26}'')/2$$
$$a_0 = (3s_{11}'' + 2s_{12}'' + 3s_{22}'' + s_{66}'')/8. \quad (4)$$

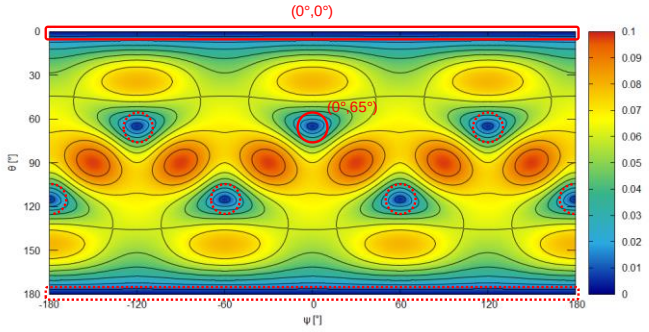

Figure 3: Coefficient of variation of s_{11}'''.

Fig. 3 shows the coefficient of variation for all angle rotations. The deep blue areas, $(\psi,\theta) = (0°,0°), (0°,65°)$ and their crystallographic equivalents satisfy the in-plane isotropic condition. The orientations are illustrated in Fig.4. In the following, the $(0°,0°)$ wafer and the $(0°,65°)$ wafer are called the Z-cut wafer and 155° rotated Y-cut (155°-Y) wafer, respectively. Between these two orientations, we chose the latter, because the electromechanical coupling coefficient k_{31} is much higher than that of the Z-cut wafer [13].

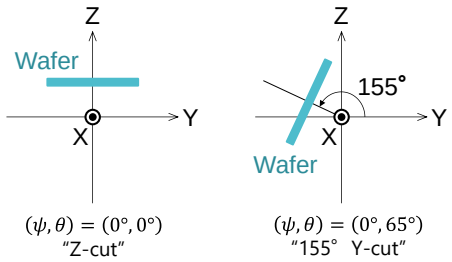

Figure 4: Wafer orientations of in-plane uniform compliance.

B. *Electrode arrangement [34]*

The matrix $\boldsymbol{d}$ for the direct piezoelectric effect was derived by rotating the matrix of the unit cell of LN, as follows;

$$\boldsymbol{d} = \begin{bmatrix} 0 & 0 & 0 & 0 & d_{15} & d_{16} \\ d_{21} & d_{22} & d_{23} & d_{24} & 0 & 0 \\ d_{31} & d_{32} & d_{33} & d_{34} & 0 & 0 \end{bmatrix}. \quad (5)$$

The 3-axis is perpendicular to the disk, and the 1-axis corresponds to that of an LN unit cell. The transverse piezoelectric coefficients d_{31} and d_{32} have different polarities of 18.4 and −25.3 pC/N, respectively, which are ideal for the wine-glass oscillation in the mode that the maximum displacement occurs along the 1-axis (0°-mode). The 0°-mode is oscillated just by applying an ac voltage between the top and bottom plane electrodes (Fig. 4a). Another wine-glass mode, in which the node is located along the 1-axis (45°-mode), is oscillated by electrodes divided into eight octants. An ac voltage is applied to each octant with a polarity opposite to those of the adjacent octants (Fig. 4b).

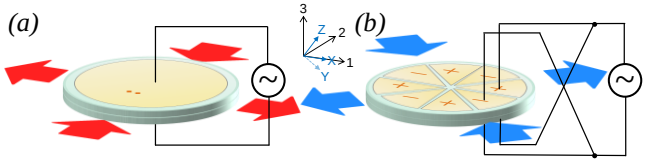

Figure 4: Transverse piezoelectricity of 155° rotated Y-cut wafer with 3-axis electrodes. (a) 0° mode. (b) 45° mode.

The specific electrode shape and dimensions for the 155°-Y cut wafer were designed by finite element analysis (FEA) (Femtet, Murata Software). Stress and piezoelectric analyses were conducted to see the distributions of stress and electrical field in the wine-glass modes. Fig. 5a shows the 1-axis strain distribution at the 0°-mode resonance. Because the stress on the inner side is much higher than that on the outer side, we decided to divide the electrodes into the inner and outer sides, and the inner-side electrodes were assigned to 0°-mode driving and sensing. The 1-axis strain distribution at the 45°-mode resonance in Fig. 5b indicate that the effectiveness of octants electrode positions. The designed electrode pattern for a disk with 25.8 mm in diameter is shown in Fig. 6. The boundary between the inner- and outer-side electrodes was decided to be 18.8 mm in diameter which was optimized by FEA. The simulated coupling coefficients of the 0° mode and 45° mode were 32.6% and 4.7%, respectively.

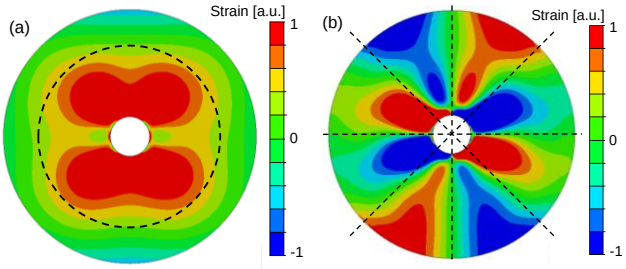

Figure 5: 1-axis strain distribution of (a) 0°-mode and (b) 45°-mode. Broken line in (a) shows boundary of inner and outer electrodes, which corresponds to high-strain area. Broken lines in (b) show boundary of octant-electrodes, which corresponds to polarity of strain.

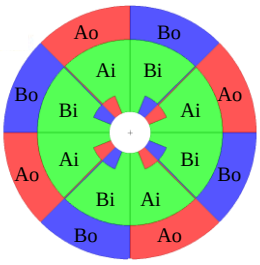

Figure 6: Electrode design. Pads are arranged near center holes for electrical connection of all 16 electrodes.

III. Experimental

A. Fabrication and assembly

The LN disk gyroscope was fabricated by double-side photolithography and grinding, as shown in Fig. 7. A four-inch 155°-Y-cut LN wafer was used. In order to decide the wafer thickness we performed modal analysis by changing it. The dots in Fig. 8 show modes near the wine-glass modes at around 95 kHz. Because disk is a thin plate, a number of flexural vibration modes exist. We chose the thickness of 330 μm, because the spurious modes are separated from the wine-glass modes. The electrode material was gold of 200 nm thickness, and 50-nm-thick chromium film was used as an adhesion film. The films were deposited using an electron beam evaporator and patterned by wet etching using gold and chromium etchants. Disks with a center hole were then cut out using a core drill machines (DAR810/DAR806, YAC DAStech).

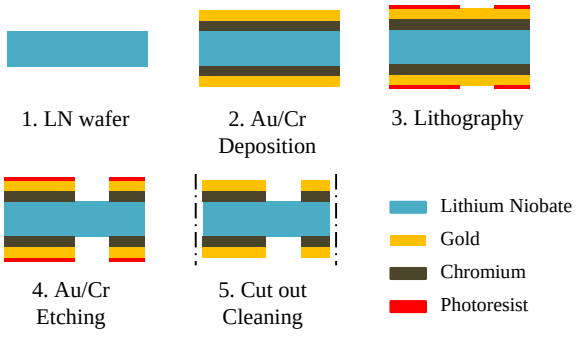

Figure 7: Process of LN disk resonator fabrication.

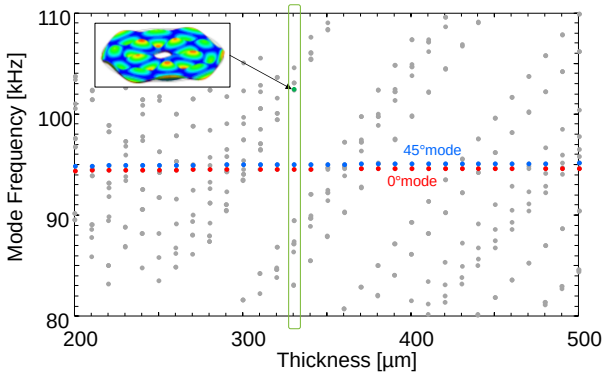

Figure 8: Mode frequencies of LN disk resonator near wine-glass mode. Inset is mode shape of one of spurious modes of 330-μm-thick disk at 102.4 kHz.

To support the disk gyroscope at the center hole and to form an electrical connection to the electrodes, we designed a custom-made socket (S.E.R. Corp.). The schematic drawing of cross section of the socket is shown in Fig. 9. The socket was made of polyetherimide, and 16 probe pins were arranged on the pad on each side of the disk. The disk was inserted to the center pillar to support the disk at the edge of the center hole. There was a window in the socket to observe the vibration of the disk resonator. The probe pins were soldered to a printed circuit board (PCB) and connected to four terminals (A_i, A_o, B_i, and B_o in Fig. 5b) on each side.

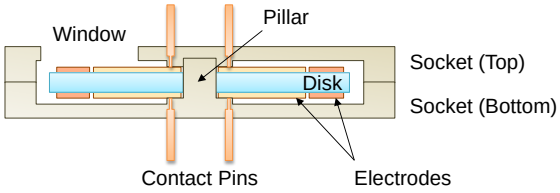

Figure 9: Cross section of custom-made socket.

B. Disk resonator characterization

The impedance spectrum of the disk was measured using an impedance analyzer (4294A, Keysite). For the 0º mode, the inner electrodes (A_i and B_i) on each side were connected and the impedance between both sides was measured. For the 45º mode, the outer electrodes (A_o) on the top and the electrodes (B_o) at the bottom were connected, and A_o at the bottom and B_o on the top were connected. The impedance between two connections were measured. In the measurement, the other electrodes that were not used were connected each other. The oscillation voltage was 500 mVrms and the spectrum near the target resonant frequency was measured. In order to extract resonator properties, the measured impedance spectrum was fitted to the simple electrical equivalent circuit model that consists of a capacitance C, inductance L, and resistance R in series, shunted by the parallel capacitance C_d.

The lateral vibration was measured using an optical heterodyne vibrometer (MLD-230D-200K, Neoark) to confirm the wine-glass-mode vibration. The same electrode connection as that in the impedance measurement was used, and the

displacement velocity was measured at the edge of the maximum displacement position in each mode.

C. Gyroscope operation

The angular rate output was demonstrated using a digital lock-in amplifier (LIA) (HF2LI, Zurich Instruments). The control schematics are shown in Fig. 10. In this measurement, no additional driving or sensing amplifier was inserted between the LIA and the disk. The input impedance of LIA was set to 50 Ω. The electrodes were connected as the same manner as described in the previous subsection. We used the 45º mode for driving and the 0º mode for Coriolis sensing, because the latter mode has larger piezoelectric output and better signal-to-noise ratio was expected. The resonant vibration in the driving mode was oscillated using the phase-locked loop (PLL) and the amplitude was maintained by auto gain control (AGC) using the PID function of the LIA. The vibration in the sensing mode was demodulated with driving signals and the rate output was obtained at an optimum phase of the demodulator [35].

The disk resonator mounted in the socket was placed on the rotation table driven by a pulse motor, and the rate output was measured at a constant rate. The zero rate output was measured to evaluate bias instability from an Allan variance plot.

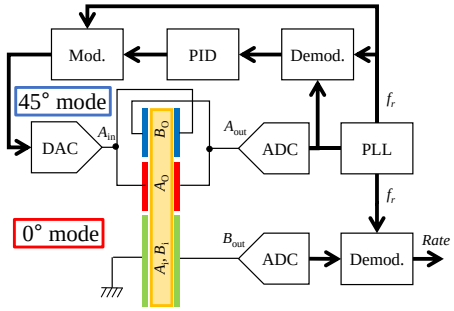

Figure 10: System diagram for angular rate measurement.

IV. Results and Discussion

A. Disk Resonator

A fabricated LN disk resonator is shown in Fig. 11. The transparent disk was almost fully covered with gold electrodes. The disk resonator was attached to the socket and the electrical connection was made through PCB. A typical impedance spectrum of the disk resonator around the wine-glass-mode frequency is plotted in Fig. 12. As designed, the resonance and anti-resonance peaks were observed near the designed resonant frequency and the resonance peaks of two wine-glass modes were matched closely. A spurious mode at about 98.4 kHz was observed. It was an out-of-plane bending mode, which was lower frequency than that of the designed value because the disk thickness was smaller than that of the design.

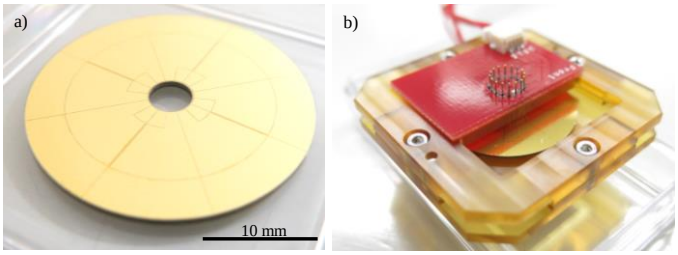

Figure 11: Fabricated disk resonator. (a) lithium niobate disk with gold electrodes and (b)assembled device with custom-made socket and PCB.

The spectra were fitted to the standard equivalent circuit for piezoelectric transducers and shown in Table 2. The properties of the device as a piezoelectric resonator were calculated from the equivalent circuit parameters and compared with the theoretical and numerical calculations, as shown in Table 3. All the parameters including resonant frequency in the wine-glass modes show good agreement. The frequency split Δf in the two modes was only 69 Hz (0.07%) in the device and the average of four measured resonators was 84 Hz.

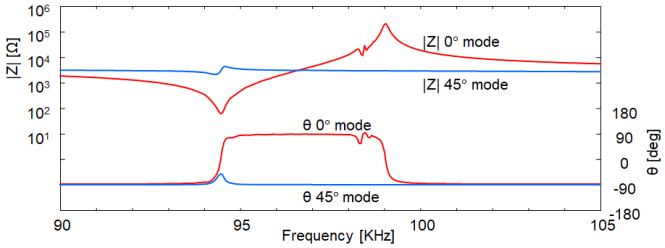

Figure 12: Impedance spectra.

Table 2: Equivalent circuit parameter in 0º and 45º modes for inner and outer electrodes, respectively.

mode	0°	45°
C_d [pF]	461.7	588.2
L [mH]	62.0	1951
C [pF]	45.8	1.46
R [Ω]	50.4	3754

The electromechanical coupling coefficients were 30.1% (0º mode) and 5.0% (45º mode), which were also in good agreement with the FEA results. We verified the proposed methods to solve the issue of the anisotropies in the elastic and piezoelectric properties of single-crystal LN, and the measured properties were found to be suitable for mode-matched wine-glass-mode gyroscopes.

Table 3: Wine-glass-mode properties.

		Exp.	FEA	Theory
f_r [kHz]	0°	94.45	94.7	95.1
	45°	94.37	95.1	95.1
Δf [Hz]		69	400	0
k [%]	0°	30.1	32.6	-
	45°	5.0	4.7	-
Q	0°	730	-	-
	45°	310	-	-

However, the Q values of these two modes were low, ranging

from 220 to 1100 in four samples. One of the reasons is the machining process. The inner and outer edges have chippings caused by grinding process whose size are about 50 μm and 10 μm, respectively. The reason of the larger chippings of the inner edge was low peripheral speed of the cylindrical grinding tool. The edge roughness caused the degradation of the Q value by two mechanism. One is the vibration energy dissipation at the roughness itself. The other is the loose contact between the socket and disk, which causes the anchor loss. The grinding tools and processing conditions should be optimized. In order to reduce the anchor loss, it is better to remove center hole. As seen in Figs. 5, the strain (displacement) at the inner edge is not small. By removing the center hole and support at the center, the anchor loss will reduced significantly. The electrical contact pins cause energy loss, so the method and position of electrical contacts should be considered to reduce the loss.

The wine-glass-mode vibration were confirmed by displacement measurement using a laser heterodyne vibrometer. The displacement amplitude at the maximum displacement point at the edge of the disk was measured in each mode and plotted as a function of driving frequency as shown in Fig. 13. For the 0º mode, the driving voltage of 200 mVp-p was applied on the inner electrodes (A_i, B_i) and the maximum displacement amplitude was 80 nm. For the 45º mode, the driving voltage of 500 mVp-p was applied on the outer electrodes (A_o, B_o) and the displacement amplitude was 25 nm.

The measured frequency split was larger than that in the electrical impedance measurement, which is caused by the impedance of the driving and sensing electronics. The stiffness of the resonator depends on the external impedance connected to the driving and sensing electrodes. It indicates that the resonant frequency of the two wine-glass modes can be tuned by connecting proper resistance.

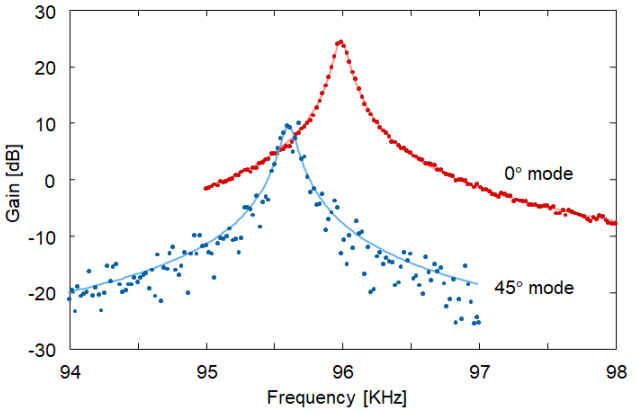

Figure 13: Lateral displacement amplitudes at each maximum displacement point of wine-glass mode.

B. *Gyroscope performances*

Fig. 14 shows the temporal rate output voltage at 30º/s for clockwise and counter clockwise rotations. The rate outputs were observed successfully, however there are some incompleteness in the output. First, the zero rate output showed random drift. This would be caused by the instable vibration of wine-glass-mode affected by the temperature, environmental vibration and electrical noises. Second, the rate output seems to contain a signal proportional to the angle position, which is the integration of the rate output. We suspect that the disk resonator unexpectedly ran in the whole-angle-mode operation since the frequency split was small but not perfectly matched. The vibration mode excited by the Coriolis effect was maintained for a certain period, which can be seen as an angle output. Therefore, on the scale factor measurement, we measured the step voltage change on applying the rotation.

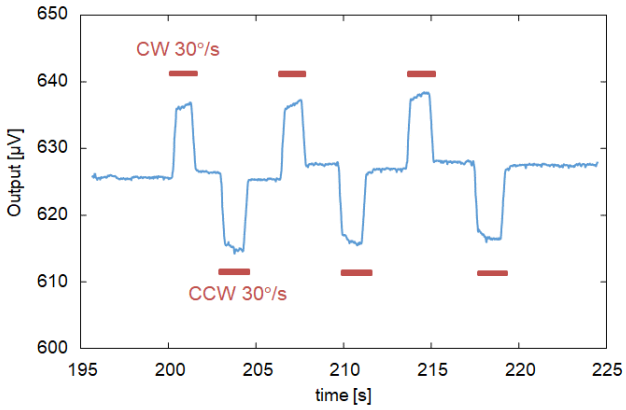

Figure 14: Temporal rate output voltage at ±30º/s rotations.

The scale factor was measured by applying constant rotations up to ±60º/s. The results are shown in Fig. 15. The output shows good linearity and the scale factor was 0.35 μV/º/s, which is relatively low, but it should be noted that no preamplifier was used in this measurement.

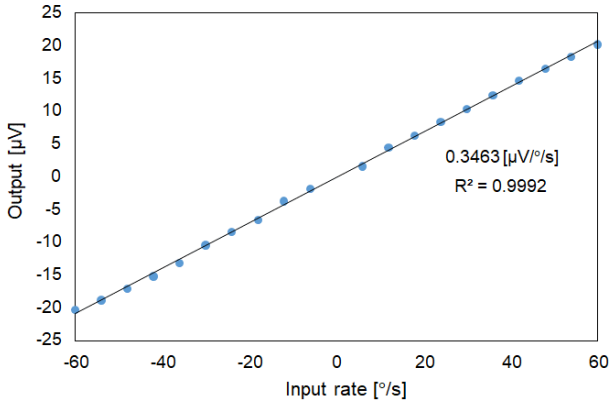

Figure 15: Scale factor plot.

The Allan variance was calculated from the rate output voltage data of 100,000 points at a sampling frequency of 224 Hz, as shown in Fig. 16. The unstable angle random walk was caused by PID control loops for PLL and AGC. The bias stability was 640º/h, comparable to that of consumer-grade MEMS gyroscopes. Since the measured quality factor was lower than expected and the resonant frequency of bulk disk resonator was intrinsically high, the decay time of the LN disk resonator is only 0.002s, which resulted in the large bias instability. In order to improve it we should consider different shape of low resonant frequency, such as cylindrical or

hemisphere shells, which is our future work.

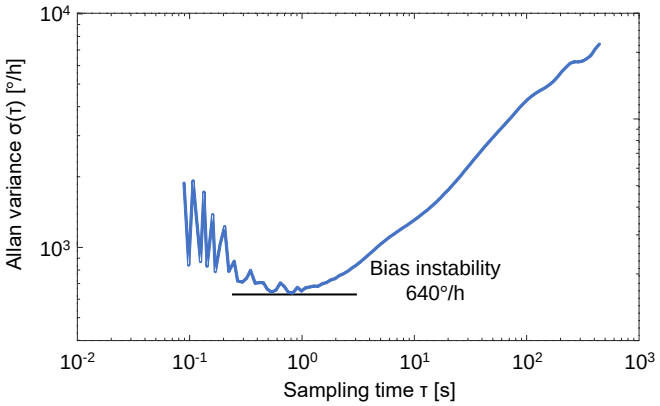

Figure 16: Allan variance plot.

This report is the first report of a wine-glass-mode gyroscope using single crystal piezoelectric lithium niobate. Although we have demonstrated the angular rate output successfully, the scale factor was still low and the bias was not stable. As we pointed out in the introduction, LN is a good piezoelectric material and single crystal LN gyroscopes have a potential of high performance. However, there are many issues to be solved. We are now working to solve them, as follows.

- Fabrication to make the device more precise with smooth surface to minimize loss in the device.
- Assembly method to minimize the anchor loss with sufficient electrical connection.
- Readout circuit for piezoelectric charge/current output and capability of frequency tuning.
- Control method suitable for disk vibratory gyroscopes.

V. Conclusion

Single-crystal LN was used for fabricating a disk resonator as a wine-glass-mode vibratory gyroscope. To realize mode matching of the two wine-glass modes, the wafer orientation was optimized and a 155°-Y-cut wafer was selected. In addition, the electrode design and voltage application scheme were proposed, and they were confirmed to operate the two modes. The disk resonator of 25.8 mm diameter and 330 μm thickness with gold electrodes was fabricated using standard photolithography and core drilling processes. The resonant frequency of the wine-glass modes was about 95 kHz and the frequency split was 0.7 % without tuning. The theoretical and numerical analysis results of the device properties as the wine-glass-mode resonator showed good agreement and were suitable for vibratory gyroscopes; however, the low Q should be improved. The closed-loop driving and open-loop detection system was used for angular rate detection using the resonator and was successfully operated. The measured scale factor was 0.35 μV/°/s and the bias instability was 640°/h.

References

[1] V. M. N. Passaro, A. Cuccovillo, L. Vaiani, M. De Carlo, and C. E. Campanella, "Gyroscope technology and applications: A review in the industrial perspective," *Sensors*, vol. 17, no. 10, p. 2284, 2017.

[2] M. F. Zaman, A. Sharma and F. Ayazi. "High Performance Matched-Mode Tuning Fork Gyroscope," in *19th IEEE International Conference on Micro Electro Mechanical Systems (MEMS)*, pp. 66–69, 2006.

[3] I. P. Prikhodko, S. Nadig, J. A. Gregory, W. A. Clark and M. W. Judy. "Half-a-month stable 0.2 degree-per-hour mode-matched MEMS gyroscope," *in 2017 IEEE International Symposium on Inertial Sensors andSystems (INERTIAL)*, pp. 1–4, Mar. 2017.

[4] J. Söderkvist, "Design of a solid-state gyroscopic sensor made of quartz," *Sensors and Actuators A: Physical*, vol. 21, Issues 1-3, p. 293-296, 1990.

[5] V. A. Hong et al., "Mode-Matching of Wineglass Mode Disk Resonator Gyroscope in (100) Single Crystal Silicon," *J. Microelectromech. Syst.*, vol. 24, no. 2, pp. 343–350, 2014.

[6] G. He, and N. Khalil, "A single-crystal silicon vibrating ring gyroscope", *in Digest Tech. Papers MEMS 2002 IEEE International Conference*, Las Vegas, January 24, 2002, pp. 718-721.

[7] I. P. Prikhodko, S. A. Zotov, A. A. Trusov, and A. M. Shkel, "Foucault pendulum on a chip: Rate integrating silicon MEMS gyroscope," *Sens. Actuat., A: Physical*, Vol. 177, pp. 67-78 (2012).

[8] C. H. Ahn, S. Nitzan, E. J. Ng, V. A. Hong, Y. Yang, T. Kimbrell, D. A. Horsley, and T. W. Kenny, "Encapsulated high frequency (235 kHz), high-Q (100 k) disk resonator gyroscope with electrostatic parametric pump," *Appl. Phys. Lett.*, Vol. 105, 243504 (2014)

[9] D. Xiao, X. Zhou, Q. Li, X. Xi, Y. Wu and X. Wu, "Design of a Disk Resonator Gyroscope With High Mechanical Sensitivity by Optimizing the Ring Thickness Distribution," *J. Microelectromech. Syst.*, vol. 25, no. 4, pp. 606-616, 2016.

[10] Q. Li, D. Xiao, X. Zhou, Y. Xu, M. Zhuo, Z. Hou, K. He, Y. Zhang, X. Wu, "0.04 degree-per-hour MEMS disk resonator gyroscope with high-quality factor (510 k) and long decaying time constant (74.9 s)," *Microsyst Nanoeng* Vol. 4, 32 (2018).

[11] F. Kulcsar, "Electromechanical properties of lead titanate zirconate ceramics modified with certain three- or five-valent additions, *J. Am. Ceram. Soc.*, vol. 47, no 7, p. 343-349, 1959.

[12] J.S. Burdess, and T. Wren, "The Theory of a Piezoelectric Disc Gyroscope", *IEEE Trans. Aerospace and Electron. Syst.*, AES-22, 4, pp. 410-418, 1986.

[13] R. S. Weis and T. K. Gaylord, "Lithium niobate: summary of physical properties and crystal structure," *Appl. Phys. A*, vol. 37, no. 4, pp. 191–203, 1985.

[14] S. Takahashi, Y. Sasaki and S. Hirose, "Driving electric field effects on piezoelectric transducers," *Jpn. J. Appl. Phys.*, vol. 36, pt. 1, no. 5B, pp. 3010-3015.

[15] K. Ono, M. Yachi, and N. Wakatsuki, "H-type single crystal piezoelectric gyroscope of an oppositely polarized $LiNbO_3$ plate," *Jpn. J. Appl. Phys.*, vol. 40, no. 5S, pp. 3699–3703, 2001.

[16] K. Nakamura and O. Masahiro, "Trapped-Energy Vibratory Gyroscopes Using Rotated Y-cut $LiNbO_3$," *Jpn. J. Appl. Phys.*, vol. 37, no. 5S, pp. 2864–2867, 1998.

[17] Y. Cheng, W. Zhang, J. Tang, D. Sun, and W. Chen, "A MEMS piezoelectric solid disk gyroscope with improved sensitivity," *Microsyst. Technol.*, vol. 21, no. 6, pp. 1371–1377, 2015.

[18] W. P. Zhang et al., "Design Optimization of BAW Micro-Piezoelectric Disk Gyroscope through Finite Element Method," *Appl. Mech. Mater.*, vol. 483, pp. 563–566, 2013.

[19] P. Taheri-Tehrani, A. D. Challoner, and D. A. Horsley, "Micromechanical Rate Integrating Gyroscope with Angle-Dependent Bias Compensation Using a Self-Precession Method," *IEEE Sens. J.*, vol. 18, no. 9, pp. 3533–3543, 2018.

[20] M. Y. Elsayed, S. Member, P. Cicek, F. Nabki, and M. N. El-gamal, "Bulk Mode Disk Resonator With Transverse Piezoelectric Actuation and Electrostatic Tuning," *J. Microelectromechanical Syst.*, vol. 25, no. 2, pp. 252–261, 2016.

[21] J. Y. Cho, J. Woo, J. Yan, R. L. Peterson, and K. Najafi, "Fused-Silica Micro Birdbath Resonator Gyroscope (μ-BRG)," J. Microelectromechanical Syst., vol. 23, no. 1, pp. 66–77, 2014.

[22] M. H. Asadian, Y. Wang and A. M. Shkel, "evelopment of 3D Fused Quartz Hemi-Toroidal Shells for High-Q Resonators and Gyroscopes," *J. Microelectromech. Syst.*, vol. 28, no. 6, pp. 954-964, 2019.

[23] D. Senkal, A. Efimovskaya, and A. M. Shkel., "Dual foucault pendulum gyroscope," in *18th International Conference on Solid-State Sensors, Actuators and Microsystems (TRANSDUCERS)*, Anchorage, AK, 2015, pp. 1219–1222.

[24] S. A. Zotov, I. P. Prikhodko, A. A. Trusov, and A. M. Shkel, "Frequency modulation based angular rate sensor," in *IEEE 24th International*

Conference on Micro Electro Mechanical Systems, Cancun, Mexico, 2011, pp. 577-580, pp. 577–580.
[25] I. P. Prikhodko, S. A. Zotov, A. A. Trusov, and A. M. Shkel, "Foucault pendulum on a chip: Rate integrating silicon MEMS gyroscope," *Sens. Actuat., A Phys.*, vol. 177, pp. 67–78, 2012.
[26] T. Tsukamoto and S. Tanaka, "Fully differential single resonator FM gyroscope using CW/CCW mode separator," *J. Microelectromech. Syst.*,27, pp. 985–994, 2018.
[27] D. D. Lynch. "MRIG frequency mismatch and quadrature control," *in 2014 International Symposium on Inertial Sensors and Systems (ISISS)*, pp. 1–4, Feb 2014.
[28] I. P. Prikhodko, J. A. Gregory, D. I. Bugrov and M. W. Judy. "Overcoming limitations of Rate Integrating Gyroscopes by virtual rotation," *in 2016 IEEE International Symposium on Inertial Sensors and Systems (INERTIAL)*, pp. 5–8, Feb. 2016.
[29] P. Taheri-Tehrani, O. Izyumin, I. Izyumin, C. H. Ahn, E. J. Ng, V. A. Hong, Y. Yang, T. W. Kenny, B. E. Boserand D. A. Horsley. "Disk resonator gyroscope with whole-angle mode operation," *in 2015 IEEE International Symposium on Inertial Sensors and Systems (ISISS) Proceedings*, pp. 1–4, Mar. 2015.
[30] Z. Hu and B. Gallacher, "Mode-matched force-rebalance control for a MEMS vibratory gyroscope," *Sens. Actuat. A. Phys.*, vol. 273, pp. 1–11, 2018.
[31] J. S. Burdess and T. Wren, "The Theory of a Piezoelectric Disc Gyroscope," *IEEE Trans. Aerosp. Electron. Syst*., vol. AES-22, no. 4, pp. 410–418, 1986.
[32] K. Obitani, T. Tsuchiya, K. Araya and M. Yachi, "Single-Crystal Lithium Niobate Piezoelectric Disk Gyroscope," *in IEEE 33rd International Conference on Micro Electro Mechanical Systems (MEMS)*, Vancouver, BC, Canada, 2020, pp. 781-784.
[33] R. T. Smith and F. S. Welsh, "Temperature Dependence of the Elastic , Piezoelectric , and Dielectric Constants of Lithium Tantalate and Lithium Niobate," *J. Appl. Phys.*, vol. 42, no. 6, pp. 2219–2230, 1971.
[34] K. Obitani, J. Qian, T. Tsuchiya, K. Araya and M. Yachi, "Electrode Design of Single Crystal Lithium Niobate Piezoelectric Disk Gyroscope," *in 2020 IEEE International Symposium on Inertial Sensors and Systems (INERTIAL)*, Hiroshima, Japan, 2020, pp. 1-2
[35] Zurich Instruments, "Application Note: Control of MEMS Coriolis Vibratory Gyroscopes," [online] Available: https://www.zhinst.com/sites/default/files/zi_appnote_mems_gyroscope.pdf

Kazutaka Obitani received the B.E. degree in engineering science and the M.E. degree in Micro Engineering from Kyoto University, Kyoto, Japan in 2018 and 2020. He studied the microfabrication technologies, mechanical properties characterization of microsystem, piezoelectric micro transducers and their application to inertial sensors.
He is currently with Sumitomo Electric Industries, Ltd., Osaka, Japan.

Kazutaka Araya received his B.S. Hachinohe Institute of Technology, Japan, in 2000. He worked with Fujitsu Media Device LTD from 2002 to 2009. In 2009, he joined tamagawa seiki co., ltd, Japan.
He is currently involved in the development and manufacture of MEMS devices and inertial measurement units.

Masanori Yachi received received his B.S. kanazawa institute of technology, Japan, in 1987. He worked with Fujitsu Limited and Fujitsu Media Device LTD from 1987 to 2002,from 2002 to 2009, respectively. In 2009, he joined tamagawa seiki co., ltd, Japan. and since 2019 he is a director in the Tamagawa mobile equipement co., ltd,, Japan.
He is currently involved in the development and manufacture of MEMS devices and inertial measurement units. He is a member of Institute of Electronics, Information and Communication Engineers.

Toshiyuki Tsuchiya (M'96) received his B.S. and M.S. degree from the University of Tokyo, Japan, and his Ph.D. degrees from Nagoya University, Japan, in 1991, 1993, and 2002, respectively. He worked with Toyota Central Research and Development Laboratories from 1993 to 2004. In 2004, he joined Kyoto University as an associate professor and since 2019 he is a professor in the Department of Micro Engineering, Kyoto University, Japan. He is currently engaged in the research of silicon surface micromachining, its application in MEMS, the mechanical property evaluation of micromaterials, and the reliability of MEMS devices.

Dr. Tsuchiya was a recipient of the R&D Awards in 1997 and the IEC 1906 Award in 2012. He is a member of MRS, the Institute of Electrical Engineers of Japan, the Japan Society of Applied Physics and the Japan Society of Mechanical Engineers.